Simulation Analysis of Force Fields in High-Power Conductive Slip Rings for Ocean Engineering

Zengwei Zhou[1], Bin Lv[1], Zemin Hu[1], Hongming Ni[1], Feng Yan[1], Yijian Wang[1]
[1]CSSC Jiujiang Jingda Technology Co., Ltd, Jiujiang 332008, Jiangxi, China
Corresponding author: Yijian Wang (e-mail: LeonChang0226@163.com)

ABSTRACT The operational stability of high-power conductive slip rings is critical for reliable power transmission and signal integrity in marine equipment such as offshore oil platforms and ships. To investigate mechanical reliability and structural stability, this study establishes a finite element simulation model of a high-power conductive slip ring for ocean engineering and designs a three-factor, four-level orthogonal experiment. Rotational speed, pressure, and friction are selected as the main influencing factors, and their stress sensitivity is determined as rotational speed > pressure > friction. The optimal parameter combination is identified as rotational speed of 5 rpm, pressure of 25 N, and friction of 7 N. Force-field simulation under the optimized conditions shows that the maximum stress occurs at the octagonal section, with a peak value of 304.994 MPa and a maximum displacement of 0.63 mm. The overall stress variation remains within a reasonable range, and structural displacement is small. The body load gradually decreases from outside to inside, consistent with the stress distribution results. The findings indicate that the structure has preliminary mechanical feasibility under the defined electromechanical load cases, while the octagonal stress-concentration region requires attention for long-term durability in high-power electromagnetic systems.

INDEX TERMS conductive slip ring, force-field simulation, orthogonal experiment, signal transmission, electromagnetic systems

I. INTRODUCTION

MARINE engineering refers to newly constructed, reconstructed, or expanded projects located seaward from the coastline, aimed at developing, utilizing, protecting, and restoring marine resources. As an application of marine engineering, electric propulsion pod thrusters are one of the most widely used propulsion methods in electric propulsion, placing the ship's power unit within an underwater pod thruster capable of rotating 360 degrees. In complex marine environments, they ensure safety, reliability, and other performance indicators, providing the maximum guarantee for overall operation [1]. Its internal structure resembles a slip ring, which is a precision transmission device that enables the transfer of signals and electrical current between two relatively rotating mechanisms [2]. It can be applied in nearly all industry sectors, including aviation, shipping, renewable energy development, and medical fields [3]. In the current industrial context, the operational stability of the overall structure is extremely important, as it affects its service life [4]. Therefore, controlling the rotational stability of the slip ring is beneficial for improving signal transmission quality and reducing wear [5,6]. The study of the stable and reliable performance of slip rings holds significant practical importance, directly impacting the operational efficiency and safety of high-power systems.

Some scholars have also applied finite element methods for research and analyzed the prediction of springback [7,8]. Pinto et al. used finite element methods to calculate modeling-related structural design methods and studied the effects of geometric shapes and the number of stiffeners on the maximum deflection of plates [9]. Qiao Ruibo et al. utilized an optimization model that is accurate and feasible, meeting the simulation requirements of complex operating conditions, which can be used to improve the simulation efficiency of electrically propelled ships [10]. Li Xin et al. pointed out that most ships use electric propulsion, characterized primarily by high ship power, which leads to diversified faults in the ship's electrical system [11]. Dong Yongqian et al. designed an orthogonal test scheme for SiC plates and summarized the process of simulating thermal deformation [12]. So far, there has been relatively little research and analysis on force field simulations of large-scale models of electric propulsion slip rings.

In order to analyze and control the structural stability of high-power conductive slip rings, this study designs an orthogonal experiment to analyze the sensitivity of various influencing factors and summarize the optimal parameter combination for structural stress minimization. Finally, the optimal parameters are used for simulation verification. The actual model is shown in Figure 1 below:

FIGURE 1. Actual Overall Slip Ring Structure

II. ESTABLISHMENT OF THE SIMULATION MODEL

A. MODEL DESIGN

The overall three-dimensional model of the high-power conductive slip ring for marine engineering is modeled according to the actual structure, as shown in Figure 2 below:

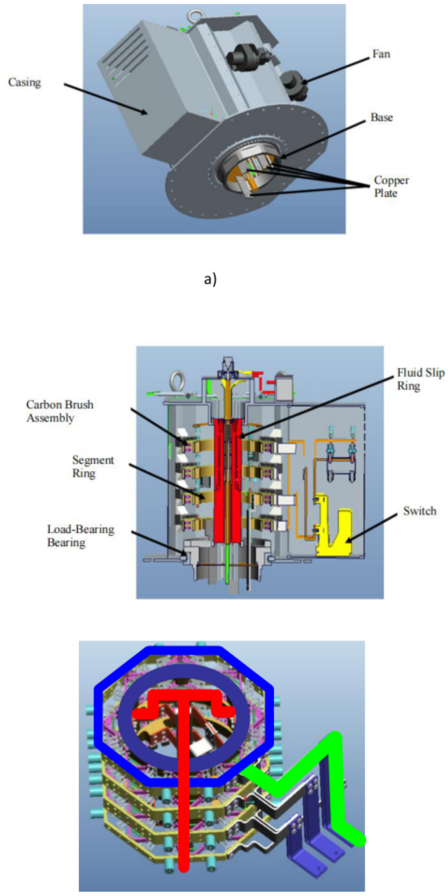

FIGURE 2. Schematic Diagram of a High-Power Slip Ring for Marine Engineering. (a) Schematic diagram of the overall model; (b) Cross-sectional view of the overall model; (c) Diagram showing the specific flow paths of the equivalent current in the overall model

The main components shown in the figure consist of the casing, fan, base, copper plate, carbon brush assembly, slip ring, load-bearing bearings, insulating non-metallic components (the green cylinder in Figure 2c), fluid slip ring (which contains signal slip rings, but these are not considered in the simulation and are therefore not labeled), and a switch. The overall model is placed vertically with the base at the bottom, providing support. During operation, the drive end (the structure within the slip ring) rotates, while the fixed end (the structure outside the slip ring) remains stationary. The contact area between the carbon brush and the slip ring experiences friction, while a certain current flows, transmitting from the fixed end to the drive end, thereby achieving signal transmission without twisting the wires.

B. 3D MODELING

Refine the details of the model. The overall height of the model, from the base to the top, is approximately 2 meters, with a width of about 2 meters, as shown in Figure 3:

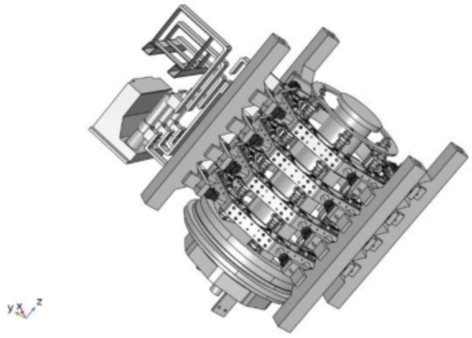

FIGURE 3. Simulation Model of High-Power Slip Ring for Marine Engineering

A finer mesh was used for meshing. The complete mesh contains 2,806,036 domain elements, 1,394,734 boundary elements, and 260,562 edge elements, as shown in Figure 4.

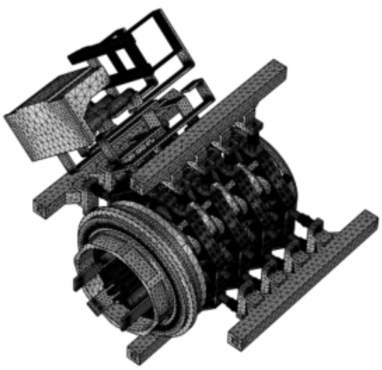

FIGURE 4. Schematic Diagram of the Overall Mesh Division of a High-Power Slip Ring for Marine Engineering

Before the simulation begins, a comprehensive model of the high-power conductive slip ring for offshore engineering is first established. The actual materials are assigned to the entire structure, with Structural Steel (Q355 grade) applied to metal parts and an engineering polymer (modeled with parameters representative of glass-fiber reinforced polyimide) applied to insulating non-metallic components, thus creating an integrated simulation model. A rotational speed is applied to the rotating end, retaining the degrees of freedom in the direction of gravity. During rotation, the simulation is influenced by body loads, namely centrifugal forces. A consistent boundary pair is set at the contact interfaces between the carbon brushes and the ring segments, with specified pressure and friction, and a steady-state analysis is conducted on the complete model.

III. SIMULATION ANALYSIS AND DISCUSSION OF RESULTS

A. ORTHOGONAL EXPERIMENTAL DESIGN

This study selects the $L_{16}(4^3)$ orthogonal array. Among the main factors affecting stress, rotational speed, pressure, and friction are chosen as orthogonal test factors, denoted as A, B, and C, respectively. Each factor is assigned four levels, and a three-factor, four-level orthogonal test scheme is designed to reasonably optimize the simulation parameters. The factor levels are shown in Table 1.

TABLE 1. Levels of Experimental Factors

Level	Test Paramenters		
	A	B	C
	Rotational Speed/rpm	Pressure/N	Friction/N
1	2	10	4
2	3	15	5
3	4	20	6
4	5	25	7

B. RESULTS AND ANALYSIS OF THE ORTHOGONAL EXPERIMENT

A statistical analysis was conducted on the stress results obtained from 16 trials, calculating the mean and range values for each level of the different indicators. The optimal level factors were selected for combination, providing the best set of simulation parameters for minimizing structural stress. Sensitivity ranking of each influencing factor was performed through range analysis. Table 2 presents the analysis of the experimental results.

Since the experimental index is stress, and kA1 > kA2 > kA3 > kA4, it can be determined that A4 is the optimal level for factor A; similarly, B4 and C4 can be calculated and determined as the optimal levels for factors B and C, respectively. Therefore, the combination of the four factors at their optimal levels, A4B4C4, represents the optimal level combination for this experiment aiming at stress minimization. By comparing the magnitude of the range R values, it is observed that RA > RB > RC, indicating that the sensitivity ranking of the influencing factors is A > B > C.

In order to intuitively analyze the variation of overall slip ring stress under different levels of rotation speed, pressure, and friction, the main effect plots of three factors (rotation speed, pressure, and friction) on stress mean values are shown in Figure 5.

TABLE 2. Analysis of Experimental Results

Item	A Rotational Speed/rpm	B Pressure/N	C Friction/N	Stress/Mpa
1	1	1	1	309.683
2	1	2	2	308.336
3	1	3	3	308.521
4	1	4	4	307.483
5	2	1	2	307.934
6	2	2	1	307.467
7	2	3	4	306.770
8	2	4	3	307.574
9	3	1	3	306.917
10	3	2	4	306.504
11	3	3	1	306.478
12	3	4	2	305.472
13	4	1	4	305.199
14	4	2	3	304.140
15	4	3	2	305.203
16	4	4	1	304.387
K1	925.536	922.239	921.147	–
K2	922.296	919.863	920.142	–
K3	919.131	920.223	920.526	Priority ranking of stress
K4	914.157	918.639	919.551	influence factors: A > B > C
k1	308.512	307.413	307.049	–
k2	307.432	306.621	306.714	–
k3	306.377	306.741	306.842	–
k4	304.719	306.213	306.517	Preferred Combination
Range R	3.793	1.200	0.532	A4B4
Preferred	A4	B4	C4	C4

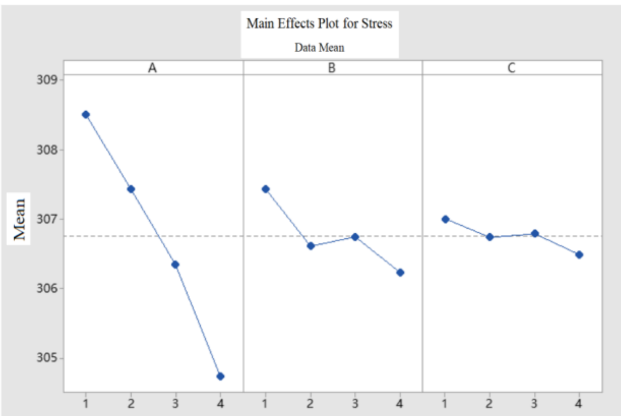

FIGURE 5. Main Effect Plot of Stress Mean

From the main effects plot of stress means, it can be observed that as the levels of factors A (rotational speed), B (pressure), and C (friction) increase, the mean values of the overall slip ring stress show a decreasing trend, indicating the presence of main effects. The steepness of the lines represents the magnitude of the main effects of the factors, and it can be seen that factor A (rotational speed) has the most significant main effect. Additionally, it can be noted that the mean indices for A4, B4, and C4 are the lowest, further confirming that the optimal combination in the experimental design for minimizing stress is: rotational speed of 5 rpm, pressure of 25 N, and friction of 7 N.

According to the calculation results, with the levels of each factor as the horizontal axis and the experimental index, namely the average stress, as the vertical axis, trend charts of each factor versus the index are plotted as shown in Figure 6. As can be seen from the figure, the average stress shows a decreasing trend with the increase of factor levels for all three factors within the defined parameter ranges. This might be attributed to complex interactions within the assembled structure. For instance, the applied contact pressure, acting through a pre-tightening mechanism, could introduce a compensatory radial compression component that partially offsets the tensile stresses induced by centrifugal force at higher rotational speeds, leading to a net reduction in the overall structural stress metric observed in the simulation.

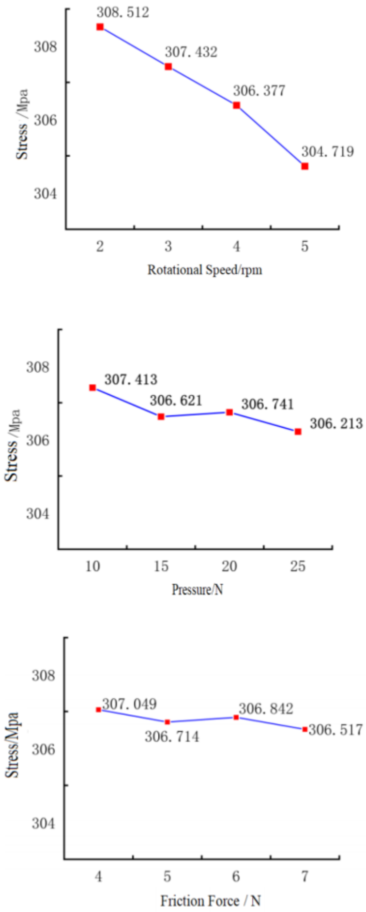

FIGURE 6. Trend Chart of Factors and Indicators

C. SIMULATION TEST

Simulation verification was carried out using the optimized parameter conditions mentioned above (rotation speed 5 rpm, pressure 25 N, and friction force 7 N), and the simulation results are shown in the figure below:

Figure 7 shows the stress distribution cloud map during the overall slip ring simulation. As can be seen from the figure, the stress shows a slight increasing trend from top to bottom, and the copper plate bend at the switch is subjected to relatively higher stress. The maximum stress is 304.994 MPa, which occurs at the octagonal section. The primary structural material is Q355 steel with a nominal yield strength of 355 MPa. While the peak stress is below the yield strength, it reaches approximately 86% of it, indicating a limited safety margin under the simulated static loads. Consideration of dynamic factors, stress concentrations, and long-term fatigue is necessary for a comprehensive safety assessment. At the same time, it can be observed that the bottom end experiences greater stress, indicating that the overall structural stress is reasonable follows a logical pattern under the applied loads.

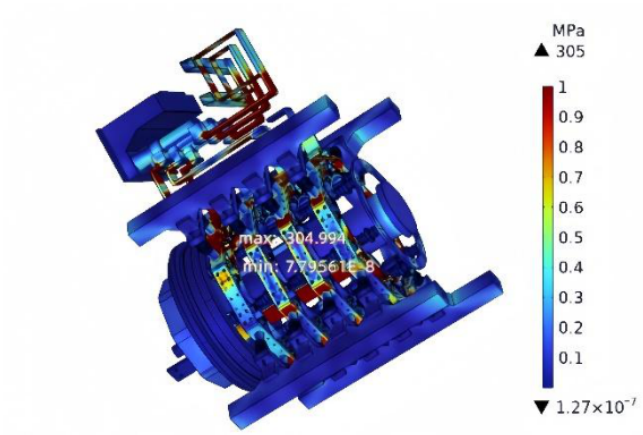

FIGURE 7. Overall Stress Distribution Cloud Diagram of the Slip Ring

Figure 8 shows the displacement distribution cloud map of the overall slip ring simulation. The copper plates at the four-ring, octagonal sections, and switches experience relatively larger displacements. The maximum displacement of the overall structure is 0.63 mm, and the minimum displacement is 0, indicating that the overall structural deformation is relatively small under the simulated conditions.

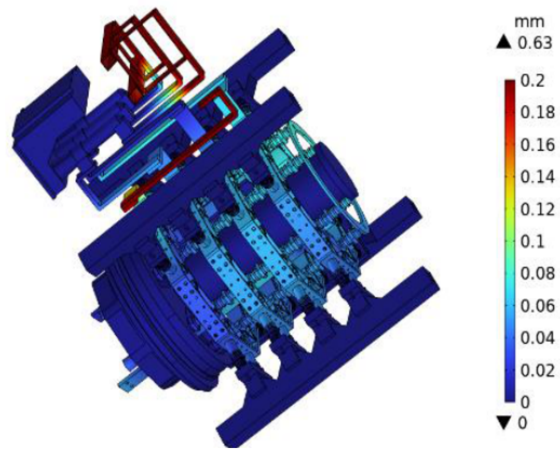

FIGURE 8. Overall Slip Ring Displacement Distribution Cloud Map

Figures 9 and 10 show the cloud diagrams of the magnitude and direction distribution of the overall slip ring body load, as well as the distribution of rotational directions when the overall structure rotates at the rotating end. In Figure 9, the length of the arrows represents the magnitude of the force. It can be seen that the body load (centrifugal force) gradually decreases from the outside to the inside, and the direction of gravity is downward. The above results correspond to the stress results, indicating that the simulation results are reliable.

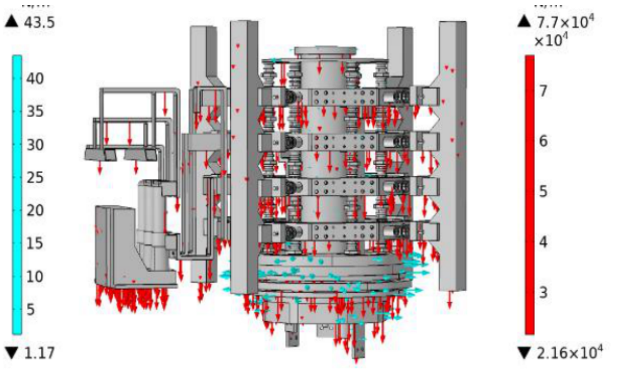

FIGURE 9. Cloud diagram of the overall slip ring showing gravity (red arrows) and centrifugal force (green arrows) distribution

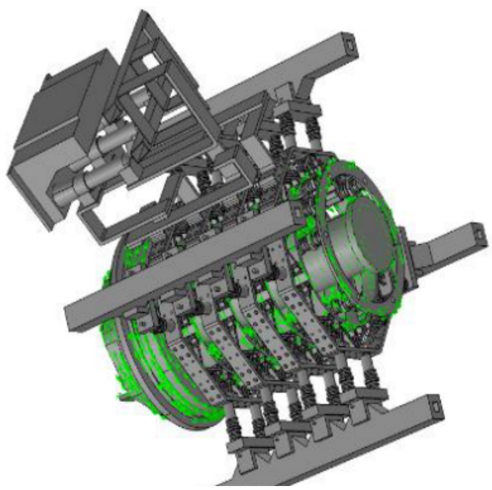

FIGURE 10. Overall Slip Ring Rotational Speed Direction Distribution Cloud Map

D. DISCUSSION ON OPTIMIZATION CRITERIA AND LIMITATIONS

The orthogonal experiment aimed to identify parameters minimizing the overall structural stress. It is important to note that this constitutes a preliminary mechanical optimization. In practical marine applications, the optimal operational parameters for a slip ring must balance multiple criteria, including electrical contact reliability (which requires sufficient pressure), wear rate, thermal management, and mechanical integrity. A parameter set yielding minimal structural stress might not be optimal for maintaining low and stable contact resistance. Therefore, the results presented here should be interpreted as identifying a mechanically favorable parameter set, which should be integrated with electrical performance tests in subsequent stages of design refinement.

Furthermore, the observed trend where increased contact pressure and friction correlate with reduced overall structural stress in the simulation merits discussion. As hypothesized earlier, this counter-intuitive result may stem from the specific load-bearing mechanism of the assembly. The preload from the contact pressure may alter the internal stress state, particularly counteracting tensile components. However, it is crucial to distinguish between overall structural stress and localized contact stress. While the former metric may decrease, the latter at the brush-ring interface is expected to increase with higher pressure and friction, potentially affecting wear and electrical performance. This study focused on the global structural response; a separate analysis of the contact micro-region is recommended for future work.

IV. CONCLUSION

A three-dimensional model of the entire high-power conductive slip ring for marine engineering was developed, informed by the structure used in actual marine applications and designed to ensure that each transmission process remains unaffected. Through an orthogonal experiment with three factors and four levels, the sensitivity of stress influence factors was determined as follows: rotational speed > pressure > friction. The optimal combination parameters for structural stress minimization were identified as: rotational speed 5 rpm, pressure 25 N, and friction 7 N. These optimal parameters were then applied in a force field simulation. The results indicate that the maximum stress in the overall structure occurs at the octagonal section, with a maximum value of 304.994 MPa, and the maximum displacement is 0.63 mm. Under the simulated static conditions, the overall stress variation is within an acceptable range, and the overall displacement deformation is relatively small. It was also observed that the body load gradually decreases from the exterior to the interior, corresponding with the stress results. This indicates that the overall structural design demonstrates preliminary mechanical feasibility under the specified loads. However, the stress level at the octagonal section suggests a need for design refinement, such as adding fillets to reduce stress concentration, or material upgrade for enhanced safety margin in dynamic ocean environments.

AUTHOR CONTRIBUTIONS

Conceptualization – Zengwei Zhou, Bin Lv, Hongming Ni, Zemin Hu, Feng Yan and Yijian Wang; methodology – Zengwei Zhou, Bin Lv, Zemin Hu, Feng Yan and Yijian Wang; investigation – Zengwei Zhou, Bin Lv, Hongming Ni, Zemin Hu, Feng Yan and Yijian Wang; writing-original draft preparation – Zengwei Zhou, Bin Lv, Hongming Ni, Zemin Hu, Feng Yan and Yijian Wang. All authors have read and agreed to the published version of the manuscript.

CONFLICTS OF INTEREST

The authors declare no conflict of interest.

FUNDING

This research was supported by, Jiangxi Province "Ganpo Juncai" Support Program-Leading Academic and Technological Leaders in Key Disciplines. (Project Number: 20243BCE51183).

ACKNOWLEDGEMENTS

Not applicable.

REFERENCES

[1] T. Xie, “A brief analysis of the importance of hybrid media slip rings in electric propulsion pod propulsors,” Shandong Industrial Technology, vol. 286, no. 8, pp. 29, 2019, doi: 10.16640/j.cnki.37-1222/t.2019.08.025.

[2] J. Lu, L. Xing, Y. Li, and F. Ge, “The key technology and developing trend of the precision conductive slip-ring,” Navigation and Control, vol. 14, no. 1, pp. 20-26, 2015, doi: 10.3969/j.issn.1674-5558.2015.01.004.

[3] W. Li, H. Fu, and F. Zhang, “A long-life conductive slip ring facilitating centroid balancing,” Science and Technology Innovation and Application, vol. 302, no. 10, pp. 92-93, 2020, doi: 10.19981/j.cn23-1581/g3.2020.10.035.

[4] H. Ma, H. Wu, and W. Yang, “Troubleshooting and emergency strategies for single-channel abnormalities in shipborne radar conductive slip rings,” Precision Manufacturing and Automation, vol. 213, no. 1, pp. 1-3, 51, 2018, doi: 10.16371/j.cnki.issn1009-962x.2018.01.001.

[5] C. Li, C. Li, T. Zhang, Y. Dong, G. Jing, X. Wang, et al., “Research on the factors affecting the wear life of slip rings in low Earth orbit satellites,” Shanghai Aerospace, vol. 36, no. S2, pp. 79-83, 2019, doi: 10.19328/j.cnki.1006-1630.2019.S.013.

[6] X. Liu, Y. Zhu, H. Liu, L. Zhao, and Z. Xie, “Reliability Evaluation of Transmission for Spaceborne Long-Life Electrical Slip Rings,” Optics and Precision Engineering, vol. 27, no. 09, pp. 2028-2035, 2019.

[7] N. A. Razali, S. H. Chung, W. J. Chung, and M. S. Joun, “Implicit elasto-plastic finite element analysis of tube-bending with an emphasis on springback prediction,” The International Journal of Advanced Manufacturing Technology, vol. 120, no. 9, pp. 6377-6391, 2022, doi: 10.1007/s00170-022-09073-8.

[8] M. Joo, M. S. Wi, S. Y. Yoon, S. Y. Lee, F. Barlat, C. N. Tome, et al., “A crystal plasticity finite element analysis on the effect of prestrain on springback,” International Journal of Mechanical Sciences, vol. 237, 107796, 2023, doi: 10.1016/j.ijmecsci.2022.107796.

[9] V. T. Pinto, M. L. Cunha, K. L. Martins, L. A. O. Rocha, M. V. Real, E. D. Santos, et al., “Geometric evaluation of steel plates subjected to uniform transverse load with rectangular or trapezoidal stiffeners by means constructal design method,” International Journal of Hydromechatronics, vol. 3, no. 2, pp. 190-198, 2020, doi: 10.1504/IJHM.2020.107788.

[10] R. Qiao, Y. Liu, and W. Zhuang, “Simulation optimization strategy for ship electric propulsion systems,” Ship Science and Technology, vol. 45, no. 7, pp. 132-137, 2023, doi: 10.3404/j.issn.1672-7649.2023.07.025.

[11] X. Li, S. Zhang, and Z. Zhang, “Case study of total power failure on a newly built electric-propelled ship,” Navigation Technology, vol. 259, no. 1, pp. 51-55, 2023.

[12] Y. Dong, H. Ma, W. Li, and W. Yang, “Simulation analysis of thermal deformation of SiC plates based on orthogonal experiment,” Electronic Process Technology, vol. 43, no. 6, pp. 330-333, 2022, doi: 10.14176/j.issn.1001-3474.2022.06.006.